Few-Body Syst (2023) 64:27
https://doi.org/10.1007/s00601-023-01813-0

Mauricio Narciso Ferreira

Evidence of the Schwinger Mechanism from Lattice QCD

Received: 16 April 2023 / Accepted: 28 April 2023 / Published online: 15 May 2023

Abstract In quantum chromodynamics (QCD), gluons acquire a mass scale through the action of the Schwinger mechanism. This mass emerges as a result of the dynamical formation of massless bound-states of gluons which manifest as longitudinally coupled poles in the vertices. In this contribution, we show how the presence of these poles can be determined from lattice QCD results for the propagators and vertices. The crucial observation that allows this determination is that the Schwinger mechanism poles induce modifications, called "displacements", to the Ward identities (WIs) relating two- and three-point functions. Importantly, the displacement functions correspond precisely to the Bethe–Salpeter amplitudes of the massless bound-states. We apply this idea to the case of the three-gluon vertex in pure Yang–Mills SU(3). Using lattice results in the corresponding WI, we find an unequivocal displacement and show that it is consistent with the prediction based on the Bethe–Salpeter equation.

1 Introduction

One of the most celebrated features of quantum chromodynamics (QCD) [1] is the emergent hadron mass (EHM) [2–9], i.e., the nonperturbative generation of massive hadrons out of fundamental fields, gluons and quarks, that are massless at the level of the Lagrangian. In this context, crucial signals of EHM have been revealed in the infrared behavior of the QCD propagators and vertices through the synergy between gauge-fixed lattice simulations [10–54] and continuum Schwinger function methods (CSM) [3,8,9,55–59], such as Schwinger–Dyson equations (SDEs) [60–71] and the functional renormalization group [72–82]. In particular, it is now established that the gluon propagator saturates to a finite value at the origin [16–19,22–33,43,47,83], which is an unequivocal signal of the dynamical generation of a gluon mass scale proposed decades ago [84–89].

Gluon mass generation has far-reaching implications. For instance, it prevents QCD from developing a Landau pole, causes the effective decoupling of gluonic modes beyond a maximum gluon wavelength [90], and suppresses Gribov copies [66,91,92]. Moreover, it sets a scale for many other dimensionful quantities, such as glueball masses [93–97]. The importance of gluon mass generation has thus prompted an intense effort to elucidate the mechanism behind its dynamical origin.

The notion that gauge bosons can acquire masses dynamically, without violating gauge symmetry, originated with Schwinger in the sixties [98,99] and has been studied in various contexts since [7,86,100–118]. In the particular case of QCD, the activation of the Schwinger mechanism for gluon mass generation hinges on the dynamical formation of massless, color-carrying, bound-states of gluons [7,68,108,110,113,114,116–118]. Such massless bound-states appear as poles in the interaction vertices, which, in turn, lead to the saturation of the propagator.

M. N. Ferreira (✉)
Department of Theoretical Physics and IFIC, University of Valencia and CSIC, 46100 Valencia, Spain
E-mail: ansonar@uv.es

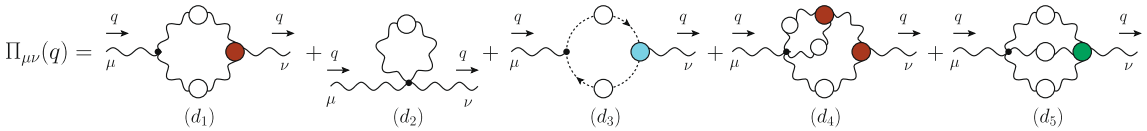

Fig. 1 Diagrammatic representation of the gluon self-energy, $\Pi_{\mu\nu}(q)$. In all our diagrams, wavy and dashed lines represent gluon and ghost fields, respectively, while circles denote dressed propagators and vertices. Feynman rules appropriate to our conventions are given in Appendix B of [64]

A difficulty that arises in the quest to confirm the occurrence of the Schwinger mechanism in QCD is that lattice simulations can only compute transverse projections of the interaction vertices [12,13,20,34,35,37,47,50,52]. However, the Schwinger mechanism poles in the vertices are strictly longitudinally coupled [7,68,107,110,113,114,116–118], and thus cannot be directly seen in lattice results for the vertex functions.

Recently [116,117], a method for confirming the existence of Schwinger mechanism poles from lattice QCD has been put forth. This method is based on the observation that the massless vertex poles induce crucial modifications to the Ward identities (WIs) relating propagators and vertices. These modifications, called "displacements", consist of the appearance of the Bethe–Salpeter (BS) amplitudes of the bound-states in the identities [7,68,113,118], in addition to the propagators and pole-free vertex parts that are present with or without the Schwinger mechanism. Hence, since the propagators and pole-free vertex parts are accessible to lattice simulations, the combination of lattice results for these quantities into the WIs allows us to determine the BS amplitude. Then, if the latter is found to be nonzero, the method allows us to confirm the occurrence of the Schwinger mechanism.

In the present contribution, we provide in Sect. 2 a brief overview of the Schwinger mechanism and its realization in QCD through the formation of massless poles in the vertices. For simplicity, we neglect the effect of dynamical quarks, focusing instead on the pure Yang–Mills SU(3). Next, in Sect. 3 we illustrate through the case of an Abelian vertex how such massless poles displace the usual WIs. There we also present the WI displacement for the three-gluon vertex, which will allow us to determine the BS amplitude of the three-gluon vertex massless pole from lattice ingredients. Then, in Sect. 4, we discuss the determination of the function $\mathcal{W}(r)$, which is a special derivative of the ghost-gluon kernel and appears in the three-gluon vertex WI displacement. In Sect. 5 we use the results of the previous sections to determine the BS amplitude, analyzing the statistical significance of the result and comparing it to the theoretical prediction obtained directly from the Bethe–Salpeter equation (BSE). Finally, in Sect. 6 we present our conclusions.

2 Overview of the Schwinger Mechanism

In the Landau gauge, which will be used throughout this work, the gluon propagator can be written as $\Delta^{ab}_{\mu\nu}(q) = -i\delta^{ab}\Delta(q)P_{\mu\nu}(q)$, where $P_{\mu\nu}(q) := g_{\mu\nu} - q_\mu q_\nu/q^2$ is the transverse projector.

The gluon propagator is determined in terms of the self-energy, $\Pi_{\mu\nu}(q)$, given diagrammatically in Fig. 1. Gauge symmetry requires that $\Pi_{\mu\nu}(q) = q^2\mathbf{\Pi}(q)P_{\mu\nu}(q)$, where $\mathbf{\Pi}(q)$ defines the dimensionless vacuum polarization. Then,

$$\Delta^{-1}(q) = q^2[1 + i\,\Pi(q)]. \tag{1}$$

The emergence of a gluon mass is signaled by the saturation of $\Delta(0)$ to a finite value, illustrated in Fig. 2 with recent lattice data from Ref. [51].

The Schwinger mechanism is based on the observation that if the vacuum polarization acquires a pole at zero momentum transfer $\Delta(0)$ will saturate, even though no gluon mass term appears in the Lagrangian. Indeed, in the presence of such a pole Eq. (1) has the limit

$$\lim_{q\to 0} i\,\mathbf{\Pi}(q) = m^2/q^2 \implies \lim_{q\to 0}\Delta^{-1}(q) = \lim_{q\to 0}(q^2+m^2) \implies \Delta^{-1}(0) = m^2, \tag{2}$$

written here in Euclidean space.

The mechanism leading to the emergence of a pole in $\mathbf{\Pi}(0)$ can vary for different theories, see e.g., [100,101]. For Yang–Mills theories, an elegant nonperturbative mechanism has been put forward which is based on the formation of a special kind of bound-state of gluons [7,68,86,103,104,106–111,113,114,116,118,119]. This mechanism can be outlined through the following sequence of ideas:

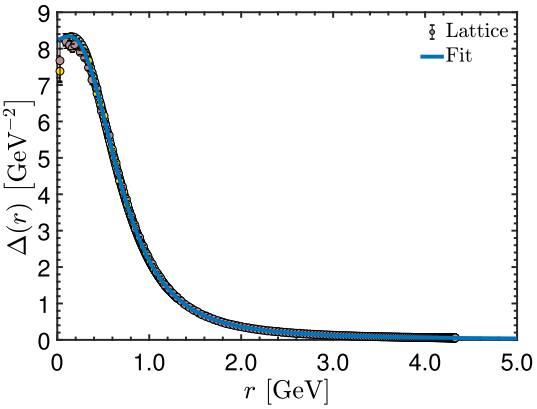

Fig. 2 Lattice data (points) from Ref. [51] for the gluon propagator, compared to a physically motivated fit given by Eq. (C11) of [116] (blue solid)

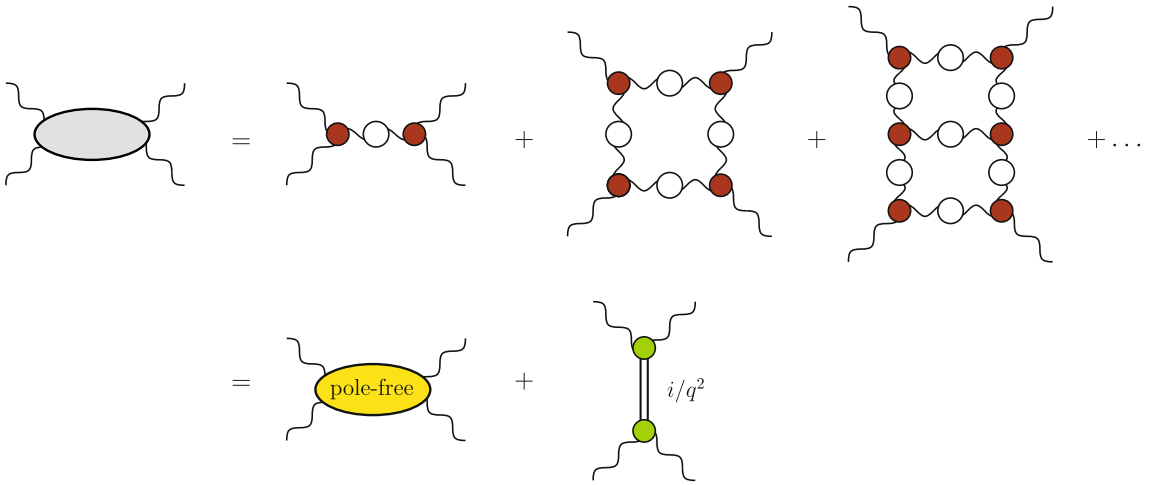

Fig. 3 Diagrammatic representation of the emergence of massless poles in the gluon–gluon scattering kernel. This kernel is one-particle irreducible with respect to vertical cuts. The first line shows some of the infinitely many diagrams contributing to the kernel. This tower of interactions is assumed to lead to the formation of a massless bound-state, with propagator i/q^2, such that the kernel acquires a pole-free and a pole contribution

(i) First, it is assumed that the gluon self-interaction is strong enough to form massless colored bound-states. These bound-states can be shown to not appear in S-matrix elements, such that no new massless particle is introduced in the spectrum of the theory [7,100,101,103,104,108]. Nevertheless, the bound-state propagator, i/q^2, induces a pole in a certain gluon–gluon scattering kernel, illustrated diagrammatically in Fig. 3.

(ii) Consequently, the fundamental vertices of the theory acquire poles at zero momentum transfer. This can be clearly seen in the case of the three-gluon vertex by analyzing the SDE that governs its momentum evolution, shown in Fig. 4. Indeed, in that equation appears the aforementioned gluon–gluon scattering kernel, which induces a pole in the vertex.

(iii) Finally, the massless poles in the vertices make their way naturally into the vacuum polarization, thus activating the Schwinger mechanism.

From now on we will focus on the three-gluon vertex, whose associated massless bound-state pole is expected to be the leading contributor to gluon mass generation [107,116,117,120,121]. We denote this vertex by $I\!\Gamma^{amn}_{\alpha\mu\nu}(q,r,p) = gf^{amn}I\!\Gamma_{\alpha\mu\nu}(q,r,p)$, where g is the gauge coupling and f^{amn} are the SU(3) structure constants.

The emergence of massless bound-state transitions in the three-gluon vertex prompts us to split $I\!\Gamma_{\alpha\mu\nu}(q,r,p)$ into a pole-free part, $\Gamma_{\alpha\mu\nu}(q,r,p)$, and a pole contribution, $V_{\alpha\mu\nu}(q,r,p)$, i.e.,

$$I\!\Gamma_{\alpha\mu\nu}(q,r,p) = \Gamma_{\alpha\mu\nu}(q,r,p) + V_{\alpha\mu\nu}(q,r,p). \tag{3}$$

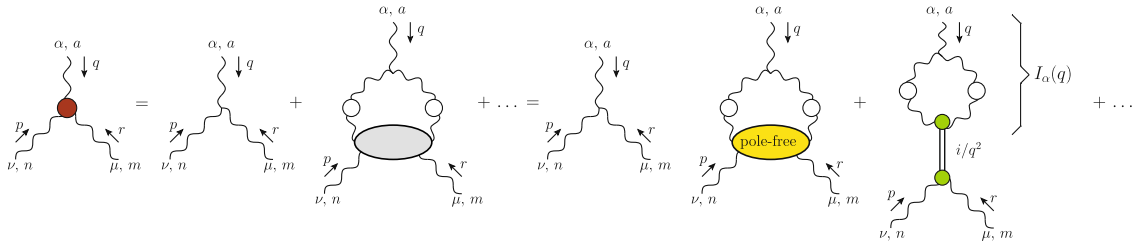

Fig. 4 Diagrammatic representation of the Schwinger-Dyson equation (SDE) for the three-gluon vertex, where appears the gluon–gluon scattering kernel of Fig. 3. The bracket defines the amplitude, $I_\alpha(q)$, for a gluon to transition to a massless bound-state. Note that, by Bose symmetry, there must also exist poles in the r and p channels, which are not shown. The ellipsis denotes additional diagrams that are omitted for simplicity

The dynamical origin of $V_{\alpha\mu\nu}(q, r, p)$ in the formation of massless poles imposes a crucial constraint on its Lorentz structures. Specifically, by Lorentz symmetry, the amplitude $I_\alpha(q)$ for a gluon to transition to a massless bound-state, defined by the bracket in Fig. 4, must be of the form $I_\alpha(q) = q_\alpha I(q)$, for some scalar $I(q)$. Hence, the $q = 0$ pole in the vertex must be associated with tensor structures longitudinal to the leg carrying momentum q. Similar considerations show that the poles at $r = 0$ and $p = 0$ must be associated with tensors longitudinal to r_μ and p_ν, respectively. Therefore, the massless poles that trigger the Schwinger mechanism must be strictly longitudinally coupled, such that [108,110]

$$P^{\alpha}_{\alpha'}(q) P^{\mu}_{\mu'}(r) P^{\nu}_{\nu'}(p) V_{\alpha\mu\nu}(q, r, p) = 0. \tag{4}$$

From Eq. (4), together with Bose symmetry of the vertex, we see that the pole part $V_{\alpha\mu\nu}(q, r, p)$ can be written as

$$V_{\alpha\mu\nu}(q, r, p) = \left(\frac{q_\alpha}{q^2}\right) C_{\mu\nu}(q, r, p) + \left(\frac{r_\mu}{r^2}\right) C_{\nu\alpha}(r, p, q) + \left(\frac{p_\nu}{p^2}\right) C_{\alpha\mu}(p, q, r), \tag{5}$$

with

$$C_{\mu\nu}(q, r, p) = C_1 g_{\mu\nu} + C_2 r_\mu r_\nu + C_3 p_\mu p_\nu + C_4 r_\mu p_\nu + C_5 p_\mu r_\nu, \tag{6}$$

where $C_i \equiv C_i(q, r, p)$. Due to the transversality of the Landau gauge gluon propagator, the form factors $C_{2,3,4}$ decouple in most calculations. Moreover, in this gauge, the form factor C_5 can be shown to not contribute to the gluon mass [108,110,116]. Hence, we will restrict our discussion to C_1.

At this point, we emphasize that the massless bound-state that triggers the Schwinger mechanism in QCD is not put in by hand, but emerges dynamically. Indeed, as with any other bound-state, its formation is governed by a BSE [7,108,110,116,118,121], represented diagrammatically in the left panel of Fig. 5.

The function that plays the role of BS amplitude in the BSE of Fig. 5 is denoted by $\mathbb{C}(r)$ and is related to the form factor C_1 defined in Eqs. (5) and (6). Specifically, note that Bose symmetry requires $C_1(q, r, p) = -C_1(q, p, r)$, such that

$$C_1(0, r, -r) = 0. \tag{7}$$

Then, in the vicinity of the $q = 0$ pole,

$$C_1(q, r, p) = 2(q \cdot r)\mathbb{C}(r), \qquad \mathbb{C}(r) := \left.\frac{\partial C_1(q, r, p)}{\partial p^2}\right|_{q=0}. \tag{8}$$

The vital first test of the Schwinger mechanism is the existence of nontrivial solutions for $\mathbb{C}(r)$. Indeed, previous studies have shown that the BSE of Fig. 5 admits nontrivial solutions, using lattice inputs for the propagator and three-gluon vertex therein [7,108,110,116,118,121]. The most up-to-date solution was obtained in Ref. [116] and is shown in the right panel of Fig. 5. For later convenience, this solution is denoted by $\mathbb{C}_\star(r)$, to distinguish it from the $\mathbb{C}(r)$ that will be determined in Sect. 5 from the WI displacement. Note that, since the BSE of Fig. 5 is a homogeneous equation, it only determines $\mathbb{C}_\star(r)$ up to a multiplicative constant; the particular solution shown there has its scale set by matching it to the result obtained in Sect. 5, as explained therein.

To conclude this section, we remark that coupling the poles of the three-gluon and ghost-gluon vertices does not significantly affect the solution shown Fig. 5. Moreover, the pole associated with the ghost-gluon vertex is subleading in comparison to $\mathbb{C}(r)$ [116,121].

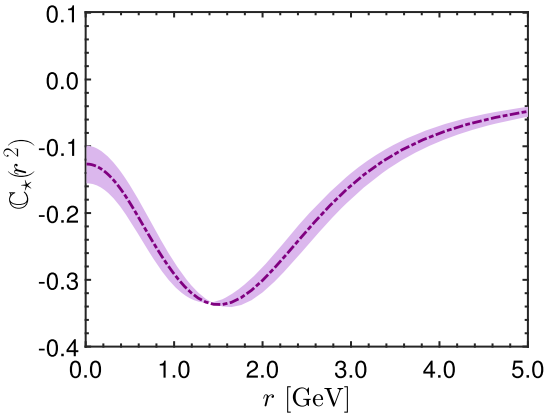

Fig. 5 Left: Bethe–Salpeter equation (BSE) governing the formation of the massless bound-state that triggers the Schwinger mechanism. The ellipsis denotes higher-order corrections to the gluon–gluon scattering kernel and coupling to poles in vertices other than the three-gluon [7,108,110,116,118,121]. Right: Bethe–Salpter (BS) amplitude, $\mathbb{C}(r)$, obtained in [116], using the BSE of the left panel

3 Ward Identity Displacement

It follows from the longitudinality property of $V_{\alpha\mu\nu}(q, r, p)$, i.e., from Eq. (4), that the Schwinger mechanism massless poles cannot be computed on the lattice by direct simulation of the three-gluon vertex. Indeed, lattice QCD can only determine the transverse projections of the vertex functions. In particular, for the three-gluon vertex, lattice observables involve the projection $\overline{\Gamma}_{\alpha\mu\nu}(q, r, p)$, defined by [13,20,34,35,37,47,50,52]

$$\overline{\Gamma}_{\alpha\mu\nu}(q, r, p) := P^{\alpha'}_{\alpha}(q) P^{\mu'}_{\mu}(r) P^{\nu'}_{\nu}(p) \text{I}\!\Gamma_{\alpha'\mu'\nu'}(q, r, p), \tag{9}$$

rather than $\text{I}\!\Gamma_{\alpha'\mu'\nu'}(q, r, p)$ itself. Then, using Eqs. (3) and (4), we see that

$$\overline{\Gamma}_{\alpha\mu\nu}(q, r, p) = P^{\alpha'}_{\alpha}(q) P^{\mu'}_{\mu}(r) P^{\nu'}_{\nu}(p) \Gamma_{\alpha'\mu'\nu'}(q, r, p), \tag{10}$$

i.e., lattice simulations only have access to the pole-free part of the vertex.

Nevertheless, a method for determining the BS amplitude, $\mathbb{C}(r)$, from lattice results has recently been devised [116,117]. The crucial observation that enables this determination is that the BS amplitudes of the massless vertex poles appear in the WI which relate two and three-point sector functions [7,68,113,118].

To fix the ideas, consider for simplicity the ghost-gluon vertex in the background field method [122–132], denoted by $\widetilde{\Gamma}_\mu(q, r, p)$, where q, r and p stand for the gluon, antighost, and ghost momenta, respectively. This vertex satisfies a Slavnov–Taylor identity (STI) [133,134] identical in form to that of the photon-scalar vertex of scalar QED. Specifically [64,135,136],

$$q^\mu \widetilde{\Gamma}_\mu(q, r, p) = D^{-1}(p) - D^{-1}(r), \tag{11}$$

where $D^{ab}(q) = i\delta^{ab} D(q)$ denotes the ghost propagator. Note that, at tree level $\widetilde{\Gamma}_\mu(q, r, p) = (r - p)_\mu$.

Now, let us assume that $\widetilde{\Gamma}_\mu(q, r, p)$ is a pole-free function at $q = 0$. From Eq. (11), we can derive the textbook WI by expanding both sides to the first order in $q = 0$ and equating coefficients of equal orders. This procedure yields,

$$\widetilde{\Gamma}_\mu(0, r, -r) = 2 r_\mu \frac{\partial D^{-1}(r)}{\partial r^2}. \tag{12}$$

Equivalently, since Lorentz invariance implies $\widetilde{\Gamma}_\mu(0, r, -r) = r_\mu \widetilde{\mathcal{A}}(r)$, for some scalar function $\widetilde{\mathcal{A}}(r)$, Eq. (12) can be recast as

$$\widetilde{\mathcal{A}}(r) = 2 \frac{\partial D^{-1}(r)}{\partial r^2}. \tag{13}$$

Next, let us activate the Schwinger mechanism, such that the vertex acquires a pole at $q = 0$. By analogy to Eq. (3), we write

$$\widetilde{\Gamma}_\mu(q, r, p) \to \widetilde{\mathbb{\Gamma}}_\mu(q, r, p) = \widetilde{\Gamma}_\mu(q, r, p) + \frac{q_\mu}{q^2}\widetilde{C}(q, r, p), \tag{14}$$

where $\widetilde{\Gamma}_\mu(q, r, p)$ now represents the pole-free part of the vertex only, while $\widetilde{C}(q, r, p)$ is the residue of the Schwinger mechanism pole.

Since the gauge symmetry is assumed to be unbroken, the STI of Eq. (11) remains valid for the full vertex, i.e.,

$$q^\mu \widetilde{\mathbb{\Gamma}}_\mu(q, r, p) = q^\mu \widetilde{\Gamma}_\mu(q, r, p) + \widetilde{C}(q, r, p) = D^{-1}(p) - D^{-1}(r). \tag{15}$$

Then we repeat the procedure of the derivation of the WI, expanding Eq. (15) in a Taylor series around $q = 0$. At zeroth order, Eq. (15) implies

$$\widetilde{C}(0, r, -r) = 0, \tag{16}$$

which is akin to the Eq. (7), derived for the three-gluon vertex from Bose symmetry in Sect. 2.

Next, at first order we obtain

$$\widetilde{\mathcal{A}}(r) = 2\left[\frac{\partial D^{-1}(r)}{\partial r^2} - \widetilde{\mathcal{C}}(r)\right], \qquad \widetilde{\mathcal{C}}(r) := \left.\frac{\partial \widetilde{C}(q, r, p)}{\partial p^2}\right|_{q=0}. \tag{17}$$

Comparing Eqs. (13) and (17), we see that the WI for the form factor $\widetilde{\mathcal{A}}(r)$ gets modified, or "displaced", by a derivative, $\widetilde{\mathcal{C}}(r)$, of the pole residue $\widetilde{C}(q, r, p)$. Note that the above definition for $\widetilde{\mathcal{C}}(r)$ is completely analogous to the BS amplitude $\mathbb{C}(r)$ of the three-gluon vertex, defined in Eq. (8).

With Eq. (17) at hand, if the propagator $D(r)$ and the vertex form factor $\widetilde{\mathcal{A}}(r)$ are somehow known, we can compute $\widetilde{\mathcal{C}}(r)$, thus determining if the vertex has a massless bound-state pole.

The same idea can be applied to the three-gluon vertex. The only fundamental difference is the non-Abelian nature of its STI, which implies that the relevant WI and its displacement have a more complicated form that mixes gluon and ghost sector functions.

Specifically, the STI which relates the three-gluon vertex to the gluon propagator is given by [1,137–141]

$$q^\alpha \mathbb{\Gamma}_{\alpha\mu\nu}(q, r, p) = F(q)\left[\Delta^{-1}(p)P^\sigma_\nu(p)H_{\sigma\mu}(p, q, r) - \Delta^{-1}(r)P^\sigma_\mu(r)H_{\sigma\nu}(r, q, p)\right], \tag{18}$$

where $F(q)$ is the ghost dressing function, defined by $D(q) = F(q)/q^2$, and $H_{\nu\mu}(r, p, q)$ is the ghost-gluon kernel [142], which will be discussed in the next section. We point out that the ghost propagator remains massless, while its dressing function, $F(q)$, becomes finite at the origin [14,17,19,21,24,28,29,39,45,51,71,107,142–150], as shown in the left panel of Fig. 6.

The WI for the three-gluon vertex is obtained as a special case of the above STI. To derive it, one expands Eq. (18) around $q = 0$ and matches coefficients of equal orders on each side of the resulting equation. Evidently, the zeroth-order expansion leads again to Eq. (7). As for the first-order term, after a suitable projection to isolate the classical tensor structure of the three-gluon vertex, one obtains the relation (for detailed derivations see [7,116])

$$\mathbb{C}(r) = L_{sg}(r) - F(0)\left\{\frac{\mathcal{W}(r)}{r^2}\Delta^{-1}(r) + \widetilde{Z}_1\frac{d\Delta^{-1}(r)}{dr^2}\right\}. \tag{19}$$

In the above equation, the displacement of the WI is *precisely* the BS amplitude $\mathbb{C}(r)$ of the Schwinger pole of the three-gluon vertex. On the other hand, $L_{sg}(r)$ is the classical form factor of the three-gluon vertex in the soft gluon limit, defined by [50]

$$L_{sg}(r) = \left.\frac{\Gamma_0^{\alpha\mu\nu}(q, r, p)P_{\alpha\alpha'}(q)P_{\mu\mu'}(r)P_{\nu\nu'}(p)\mathbb{\Gamma}^{\alpha'\mu'\nu'}(q, r, p)}{\Gamma_0^{\alpha\mu\nu}(q, r, p)P_{\alpha\alpha'}(q)P_{\mu\mu'}(r)P_{\nu\nu'}(p)\Gamma_0^{\alpha'\mu'\nu'}(q, r, p)}\right|_{q\to 0}, \tag{20}$$

with $\Gamma_0^{\alpha\mu\nu}(q, r, p)$ denoting the tree-level form of the vertex. By now, this form factor has been extensively studied on the lattice [34,35,37,47,50,52], such that its form is rather accurately known. In the right panel of

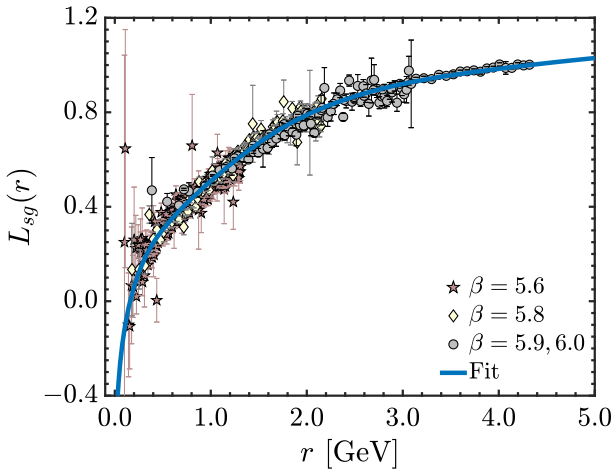

Fig. 6 Left: Lattice data (points) from Refs. [39,51] for the ghost dressing function, $F(r)$. Right: Form factor $L_{sg}(r)$ of the three-gluon vertex in the soft gluon limit obtained from lattice quantum chromodynamics (QCD) in Ref. [50] (points). The blue solid curve in each panel denotes a fit to the corresponding data, given by Eqs. (C6) and (C12) of [116], for $F(r)$ and $L_{sg}(r)$, respectively

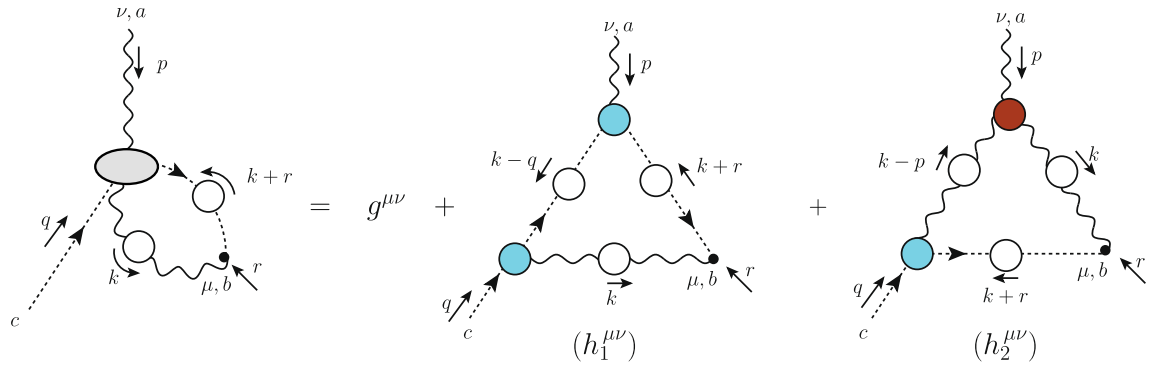

Fig. 7 SDE for the ghost–gluon scattering kernel, $H_{\mu\nu}(r, q, p)$. We omit a diagram containing a 1PI four-point function, which has been shown to contribute to the ghost-gluon vertex at the 2% level only [152]

Fig. 6 we show the lattice results for $L_{sg}(r)$ from [50] (points), together with a physically motivated fit for it given by Eq. (C12) of [116] (blue continuous curve).

Lastly, $\mathcal{W}(r)$ is a particular derivative of the ghost-gluon kernel, namely [116,151]

$$\mathcal{W}(r) = -\frac{1}{3r^2} P^{\mu\nu}(r) \left[\frac{\partial H_{\nu\mu}(p,q,r)}{\partial q^\alpha} \right]_{q=0}, \tag{21}$$

while $\widetilde{Z}_1$ is the renormalization constant of the ghost-gluon vertex. The latter is finite in the Landau gauge, by virtue of the well-known Taylor theorem [133].

The Eq. (19) is the central relation that will enable us to determine the BS amplitude, $\mathbb{C}(r)$, from lattice data for the gluon and ghost propagators and the form factor $L_{sg}(r)$ of the three-gluon vertex. To this end, we need first to determine the ghost-gluon kernel derivative $\mathcal{W}(r)$ appearing in Eq. (19).

4 Ghost-Gluon Kernel Contribution

Now we briefly describe our lattice-driven SDE determination of $\mathcal{W}(r)$. The starting point of this analysis is the SDE that defines the ghost-gluon kernel, shown diagrammatically in Fig. 7.

From that equation, the function $\mathcal{W}(r)$ can be isolated through Eq. (21). The resulting expression for $\mathcal{W}(r)$ can be written as

$$\mathcal{W}(r) = \mathcal{W}_1(r) + \mathcal{W}_2(r), \tag{22}$$

where the $\mathcal{W}_i(r)$ denote the contributions of the diagrams ($h_i^{\mu\nu}$) in Fig. 7, respectively. These are given by

$$\mathcal{W}_1(r) = \widetilde{\lambda} \int_k \Delta(k) D(k) D(k+r)(r\cdot k) f(k,r) B_1(k+r,-k,-r) B_1(k,0,-k),$$
$$\mathcal{W}_2(r) = \widetilde{\lambda} \int_k \Delta(k) \Delta(k+r) D(k+r) B_1(k+r,0,-k-r) \mathcal{I}_{\mathcal{W}}(-r,-k,k+r), \tag{23}$$

where $\widetilde{\lambda} := ig^2 C_{\rm A} \widetilde{Z}_1/6$, $C_{\rm A}$ is the Casimir eigenvalue of the adjoint representation [N for SU(N)], and

$$f(k,r) := 1 - \frac{(r\cdot k)^2}{r^2 k^2}. \tag{24}$$

In addition to the gluon and ghost propagators, $\Delta(r)$ and $D(r)$, respectively, Eq. (23) involves quantities that are related to the ghost-gluon and three-gluon vertices, namely $B_1(r,p,q)$, $\widetilde{Z}_1$ and $\mathcal{I}_{\mathcal{W}}(q,r,p)$. Below we explain their meaning in detail.

(i) In Eq. (23), $B_1(r,p,q)$ denotes the classical form factor of the ghost-gluon vertex, $\rm I\!\Gamma_\mu(r,p,q)$, whose most general tensor structure is given by

$$\rm I\!\Gamma_\mu(r,p,q) = B_1(r,p,q) r_\mu + B_2(r,p,q) q_\mu. \tag{25}$$

Hence, at tree level $B_1^0 = 1$ and $B_2^0 = 0$. Note that the ghost-gluon vertex and kernel are related by the STI

$$\rm I\!\Gamma_\mu(r,p,q) = r^\nu H_{\nu\mu}(q,r,p). \tag{26}$$

Thus, the general kinematics $B_1(r,p,q)$ can be determined through another projection of the SDE of Fig. 7. Such an SDE determination of the general kinematics $B_1(r,p,q)$ was performed in Refs. [117,118], also using lattice results as inputs for all its ingredients. It is beyond the scope of the present work to describe this analysis in detail. It suffices to mention that the results for $B_1(r,p,q)$ deviate only moderately from its tree-level value, in agreement with several previous continuum studies [71,79,142,149,150,153–157], and reproduce the available lattice data from Ref. [14,15]. As such, the impact of the precise dressing of $B_1(r,p,q)$ on the $\mathcal{W}(r)$ computed through Eq. (22) is under stringent control.

(ii) As previously mentioned, the ghost-gluon kernel, and hence $\mathcal{W}(r)$, is finite in Landau gauge [133]. Nevertheless, multiplicative renormalization of the theory leads to the appearance [151] of the ghost-gluon renormalization constant, $\widetilde{Z}_1$, in Eq. (23). The *finite* value of this constant depends on the renormalization scheme adopted. To take the most advantage of the lattice data for the propagators and the three-gluon vertex, we adopt the scheme where $\Delta(r)$, $F(r)$ and $L_{sg}(r)$ are most readily renormalized. Namely, the so-called asymmetric MOM scheme [34,37,50,51,118,151]. The latter is defined by the prescriptions

$$\Delta^{-1}(\mu^2) = \mu^2, \qquad F(\mu^2) = 1, \qquad L_{sg}(\mu^2) = 1, \tag{27}$$

where we choose $\mu = 4.3$ GeV as renormalization point. The corresponding value for the coupling is $g^2 = 4\pi\alpha_s$, with $\alpha_s(4.3\ \text{GeV}) = 0.27$, as determined in the lattice study of [37]. Within this renormalization scheme, the same SDE analysis of Refs. [117,118] used to determine $B_1(r,p,q)$ also yields the value $\widetilde{Z}_1 = 0.9333$.

(iii) Finally, $\mathcal{I}_{\mathcal{W}}(q,r,p)$ is a particular transverse projection of the three-gluon vertex, namely

$$\mathcal{I}_{\mathcal{W}}(q,r,p) := \frac{1}{2}(q-r)^\nu \overline{\Gamma}^\alpha_{\alpha\mu}(q,r,p)\,, \tag{28}$$

which encodes the total contribution of $\overline{\Gamma}^\alpha_{\alpha\mu}(q,r,p)$ to the SDE governing $\mathcal{W}(r^2)$. Note that the Bose symmetry of $\overline{\Gamma}^\alpha_{\alpha\mu}(q,r,p)$ implies

$$\mathcal{I}_{\mathcal{W}}(q,r,p) = \mathcal{I}_{\mathcal{W}}(r,q,p). \tag{29}$$

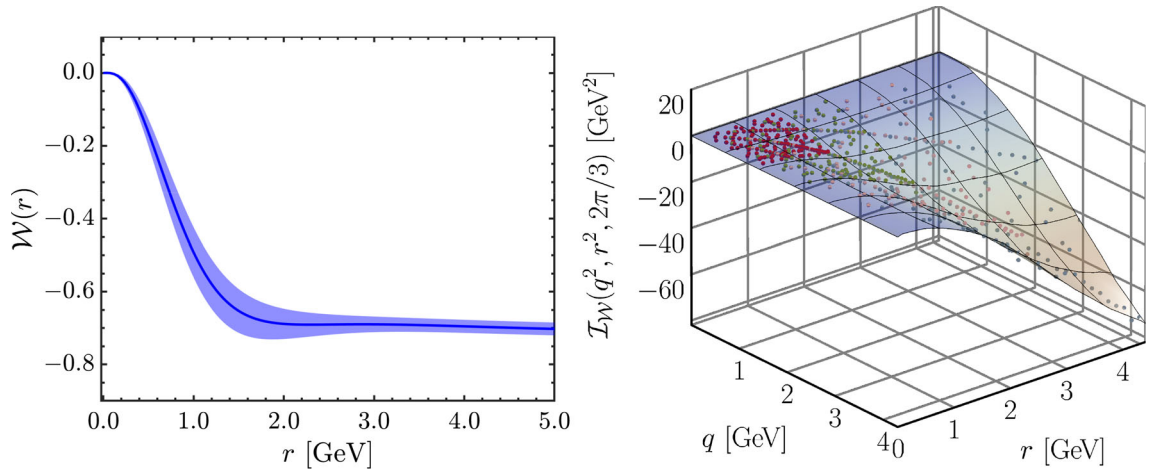

Fig. 8 Left: $\mathcal{W}(r)$ obtained using the planar degeneracy approximation of Eq. (31) for the three-gluon vertex (blue solid curve) together with uncertainty estimate (blue band) obtained by using the Neural Network predictor for $\mathcal{I}_{\mathcal{W}}$. Right: Lattice results (points) for $\mathcal{I}_{\mathcal{W}}(q, r, p)$, when the momenta q and r are at an angle of $2\pi/3$. The surface shows the result of the Neural Network predictor trained on the data points. Another value for the angle can be seen in Fig. 4 of Ref. [117]

In a series of previous works [116,151,158], the ingredient appearing in Eq. (22) that represented the largest uncertainty was $\mathcal{I}_{\mathcal{W}}(q, r, p)$. Since lattice results for the general kinematics three-gluon vertex were not available then, in those references $\mathcal{W}(r)$ had been approximated by various *Ansätze* based on the Ball-Chiu construction of the three-gluon vertex [137,156]. Recently, general kinematics lattice data for $\overline{\Gamma}_{\alpha\mu\nu}(q, r, p)$ became available [52–54], prompting a more accurate determination of $\mathcal{W}(r)$.

Remarkably the general kinematics lattice results of Refs. [52–54,117], as well as some continuum studies [159–161], revealed that a compact expression provides a rather accurate approximation for the transversely projected three-gluon vertex. Specifically,

$$\overline{\Gamma}_{\alpha\mu\nu}(q, r, p) \approx \overline{\Gamma}^{0}_{\alpha\mu\nu}(q, r, p) L_{sg}(s), \qquad s^2 := (q^2 + r^2 + p^2)/2, \tag{30}$$

where $\overline{\Gamma}^{0}_{\alpha\mu\nu}(q, r, p)$ denotes the tree-level form of $\overline{\Gamma}_{\alpha\mu\nu}(q, r, p)$.

In Eq. (30) the sole dynamical ingredient is the soft gluon form factor, $L_{sg}(r)$, of Fig. 6, which now appears evaluated at the Bose-symmetric combination of momenta given by s. Note that general kinematics form factors of the three-gluon vertex are expected to depend on three Lorentz scalars. The fact that in Eq. (30) the form factor depends only on s, whose values define planes in the coordinate system (q^2, r^2, p^2), has been termed *planar degeneracy* [52].

Using the planar degeneracy approximation of Eq. (30) into Eq. (28), we find a similarly compact expression for $\mathcal{I}_{\mathcal{W}}(q, r, p)$, namely

$$\mathcal{I}_{\mathcal{W}}(q, r, p) \approx \mathcal{I}^{0}_{\mathcal{W}}(q, r, p) L_{sg}(s), \tag{31}$$

where $\mathcal{I}^{0}_{\mathcal{W}}(q, r, p)$ is the tree-level value of $\mathcal{I}_{\mathcal{W}}$, given by

$$\mathcal{I}^{0}_{\mathcal{W}}(q, r, p) := \frac{2 f(q, r)}{p^2} \left[2q^2 r^2 - (q^2 + r^2)(q \cdot r) - (q \cdot r)^2\right]. \tag{32}$$

The Eq. (31) provides us with a baseline for computing $\mathcal{W}(r)$ accurately and expeditiously.

In order to carry out the integrations over the whole momentum space in Eq. (23), we employ fits for the lattice data for $\Delta(r)$ and $F(r)$ from [51] and for the $L_{sg}(r)$ of [47] which are constructed to reproduce the one-loop anomalous dimensions of these functions for large momenta. These fits are given in Appendix C of [116] and are all renormalized consistently in the asymmetric MOM scheme [118,151].

Using the above ingredients, combined with the results for $B_1(r, p, q)$, $\widetilde{Z}_1$ and α_s mentioned in items (i) and (ii) above, we evaluate the Euclidean form of Eq. (23) to obtain $\mathcal{W}(r)$. The result is shown as the blue solid curve in the left panel of Fig. 8.

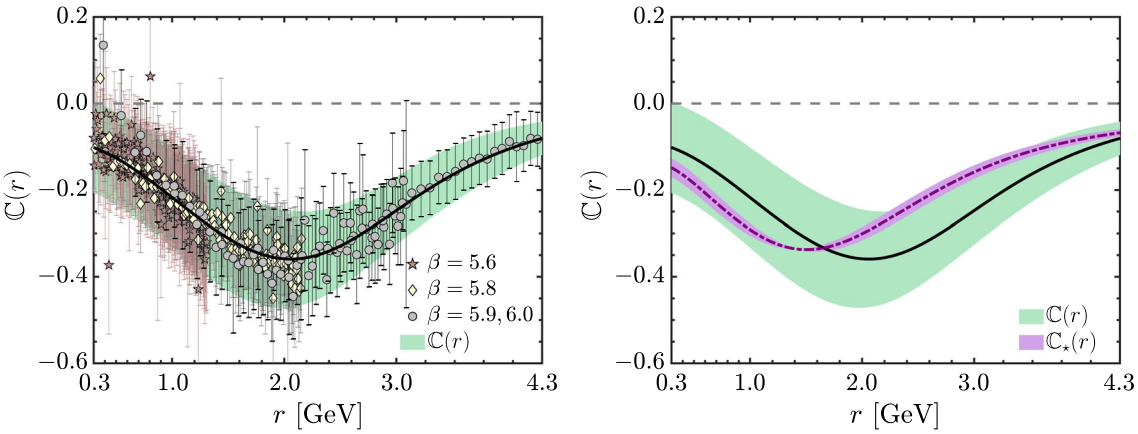

Fig. 9 Left: Result for $\mathbb{C}(r)$ obtained from the Ward identity (WI) displacement, i.e., Eq. (19). The black continuous line results from using the lattice-driven SDE result for $\mathcal{W}(r)$, shown in the right panel of Fig. 8, and fits for $\Delta(r)$, $L_{sg}(r)$ and $F(r)$. Using for $L_{sg}(r)$ the lattice data of Ref. [50] directly yields the points. The green band emphasizes the typical size of the error estimate for $\mathbb{C}(r)$ and is obtained by fitting the upper and lower bounds of the error bars of the points. Right: Comparison of the $\mathbb{C}(r)$ (black line and green band) of the left panel to the BSE prediction, $\mathbb{C}_\star(r)$, (purple dot-dashed and error band) of Ref. [116]

At this point, it is important to quantify the errors introduced in $\mathcal{W}(r)$ by the use of the approximate form of the three-gluon vertex given in Eq. (30). To that end, the projection $\mathcal{I}_{\mathcal{W}}(q, r, p)$ has been computed *directly* through lattice simulation in Ref. [117]. Results for various lattice setups are shown as points in the right panel of Fig. 8. These data correspond to momenta q and r at an angle of $2\pi/3$ and with arbitrary magnitudes. For different angles, the $\mathcal{I}_{\mathcal{W}}(q, r, p)$ is qualitatively similar.

In order to employ the lattice results for $\mathcal{I}_{\mathcal{W}}(q, r, p)$ into the SDE of $\mathcal{W}(r)$, we need a smooth interpolant. Since the data points depend on three kinematic variables (the magnitudes of two momenta and the angle between them), it is difficult to come up with a functional form that fits them accurately. Moreover, since the data is noisy, standard interpolants such as splines are unsuitable.

A reliable method to interpolate the general kinematics $\mathcal{I}_{\mathcal{W}}(q, r, p)$ consists of training a Neural Network predictor on the lattice data [117]. To this end, we randomly selected one-third of the 335,628 lattice points for $\mathcal{I}_{\mathcal{W}}(q, r, p)$ as a training set. The data was then fed into the Mathematica routine "Predict", with the option "Neural Network", which outputs a smooth predictor function. The remaining 223 725 lattice data points were then used to confirm the accuracy of the resulting interpolant, by verifying that the predicted values were always within one standard deviation of the actual lattice results [117].

In the right panel of Fig. 8, the Neural Network predictor for $\mathcal{I}_{\mathcal{W}}(q, r, p)$ is represented by the color-mapped surface, which is compared to the full set of lattice data for the angle between q and r set at $2\pi/3$. In that figure, the accuracy and smoothness of the Neural Network result are clearly seen.

The Neural Network predictor for $\mathcal{I}_{\mathcal{W}}(q, r, p)$ can then be used directly into Eq. (23), as an alternative method for computing $\mathcal{W}(r)$. Quite remarkably, the results for $\mathcal{W}(r)$ computed with this method and those obtained from the planar degeneracy approximation of Eq. (31) differ by only 2.5% [117]. Combining this estimate of the systematic error with propagated statistical error of $L_{sg}(r)$ [117] we obtain a total error budget for $\mathcal{W}(r)$, which is represented as the blue band shown in the left panel of Fig. 8.

5 Determination of the Displacement Amplitude from Lattice Inputs

Now we are in position to determine $\mathbb{C}(r)$ from the WI displacement, i.e., through Eq. (19).

Combining the blue curve for $\mathcal{W}(r)$ of Fig. 8 with the aforementioned fits for $\Delta(r)$, $F(r)$ and $L_{sg}(r)$ into Eq. (19), we obtain for $\mathbb{C}(r)$ the black solid curve in the left panel of Fig. 9. The points in the same panel show the result for $\mathbb{C}(r)$ obtained by using *directly* in Eq. (19) the lattice data points of [50] for $L_{sg}(r)$, instead of a fit.

The statistical significance of the above result for $\mathbb{C}(r)$ can be quantified by comparing it to the null hypothesis, namely $\mathbb{C} = \mathbb{C}_0 = 0$. To this end, we compute the χ^2 of our points for $\mathbb{C}(r)$, with the null

hypothesis taken as the estimator of the data, i.e.,

$$\chi^2 = \sum_{i=1}^{n_r} \frac{[\mathbb{C}(r_i) - \mathbb{C}_0(r_i)]^2}{\epsilon^2_{\mathbb{C}(r_i)}} = 2\,630. \tag{33}$$

In the above equation, $\epsilon_{\mathbb{C}(r_i)}$ denotes the error estimate of $\mathbb{C}(r_i)$ (the error bars in Fig. 9). The sum is performed over the $n_r = 515$ indices i such that $r_i \in [0.3, 4.3]$ GeV.

From the result in Eq. (33), we can compute the probability, $P_{\mathbb{C}_0}$, that our result for $\mathbb{C}(r)$ is consistent with the null hypothesis. Denoting by $\chi^2_{\rm PDF}(n_r, x)$ the χ^2 probability distribution function with $n_r = 515$ degrees of freedom, we obtain [117]

$$P_{\mathbb{C}_0} = \int_{\chi^2=2\,630}^{\infty} \chi^2_{\rm PDF}(515, x)dx = \frac{\Gamma(n_r/2, \chi^2/2)}{\Gamma(n_r/2)}\bigg|_{n_r=515}^{\chi^2=2\,630} = 7.3 \times 10^{-280}. \tag{34}$$

The vanishingly small probability obtained in Eq. (34) is to be understood as meaning that, in the absence of additional uncertainties or correlations in the data, the null hypothesis $\mathbb{C}_0$ is completely excluded. Moreover, we point out that even if the error of *every data point* for $\mathbb{C}(r)$ was 95% larger we could still discard $\mathbb{C}_0$ at the 5σ confidence level.

The result for $\mathbb{C}(r)$ obtained in this way can then be compared to the BSE prediction, $\mathbb{C}_\star(r)$, of Ref. [116], shown in the right panel of Fig. 5. To this end, we first need to determine the overall scale and sign of $\mathbb{C}_\star(r)$, which are left undetermined by the homogeneous nature of the BSE.

Denoting by $\mathbb{C}_{\rm BSE}(r)$ a solution of the homogeneous BSE, we first define

$$\mathbb{C}_\star(r) = b\,\mathbb{C}_{\rm BSE}(r), \tag{35}$$

with b a constant. Then, we determine the multiplicative constant b by minimizing the χ^2 measure for the discrepancy between $\mathbb{C}$ and $\mathbb{C}_\star$ as

$$\chi^2_\star = \sum_i \frac{[\mathbb{C}(r_i) - \mathbb{C}_\star(r_i)]^2}{\epsilon^2_{\mathbb{C}(r_i)}}. \tag{36}$$

The result of this procedure is the $\mathbb{C}_\star(r)$ shown previously in the right panel of Fig. 5.

Next, in the right panel of Fig. 9 we compare $\mathbb{C}(r)$ and $\mathbb{C}_\star(r)$ directly, finding a rather good agreement. The main difference is in the position of the minimum, which is shifted from $r = 1.93^{+0.09}_{-0.06}$ GeV for $\mathbb{C}(r)$ to $r = 1.5 \pm 0.1$ for $\mathbb{C}_\star(r)$.

Finally, in addition to determining the scale and sign of $\mathbb{C}_\star(r)$, the $\chi^2_\star$ measure of Eq. (36) allows us to perform a statistical analysis of the compatibility between the BSE prediction and the lattice result. Specifically, after setting the scale of $\mathbb{C}_\star$ we obtain $\chi^2_\star = 258.5$, which is smaller than the number of degrees of freedom. Indeed, this value of $\chi^2_\star$ translates to a near unit probability,

$$P_{\mathbb{C}_\star} = \frac{\Gamma(n_r/2, \chi^2_\star/2)}{\Gamma(n_r/2)}\bigg|_{n_r=515}^{\chi^2_\star=258.5} = 1 - 2.0 \times 10^{-23}, \tag{37}$$

of the points $\mathbb{C}(r)$ being compatible with $\mathbb{C}_\star(r)$ [118].

6 Conclusion

The displacement of the WIs by the formation of massless vertex poles is a distinctive feature of the Schwinger mechanism for gluon mass generation, which allows its verification from lattice QCD results. In the present work, we have used this framework to demonstrate that the three-gluon vertex in Yang–Mills SU(3) has such a pole. Indeed, our analysis of the WI displacement using lattice data unequivocally excludes the null hypothesis of a vanishing BS amplitude, $\mathbb{C} = 0$. Instead, our results reveal an excellent agreement between the $\mathbb{C}(r)$ derived from the WI and the BSE prediction, providing outstanding evidence for the occurrence of the Schwinger mechanism in QCD.

It is important to emphasize that while the present analysis was carried out in the simpler setting of pure Yang–Mills SU(3), the same ideas hold in the presence of dynamical quarks. In particular, the WI displacement for the three-gluon vertex retains exactly the same form as in Eq. (19) in the unquenched case, for which lattice data for the propagators and vertices also exist [16,29,45,47,162]. Indeed, a study is already underway to investigate the Schwinger mechanism poles in the presence of quarks and should be reported soon.

Finally, in the present work, we have focused entirely on the massless pole content of the three-gluon vertex. However, once the Schwinger mechanism is active, it is expected that massless poles appear in various vertices [113], since the different vertices are connected to one another through the SDEs. As such, other important signals of the Schwinger mechanism may be present in functions such as the ghost-gluon kernel, and the quark-gluon and four-gluon vertices, which are currently under investigation as well.

Acknowledgements The author thanks A.C. Aguilar, J. Papavassiliou, C.D. Roberts, and J. Rodríguez-Quintero for the collaborations.

Authors' Contributions M.N.F. is the sole author of this submission.

Funding Open Access funding provided thanks to the CRUE-CSIC agreement with Springer Nature. M.N.F. is supported by the Grant PID2020-113334GB-I00 and the contract CIAPOS/2021/74, from the Spanish MICINN and the Generalitat Valenciana, respectively.

Declarations

Conflict of interest The author has no relevant financial or non-financial interests to disclose.

References

1. W.J. Marciano, H. Pagels, Quantum chromodynamics: a review. Phys. Rep. **36**, 137 (1978). https://doi.org/10.1016/0370-1573(78)90208-9
2. C.D. Roberts, S.M. Schmidt, Reflections upon the emergence of hadronic mass. Eur. Phys. J. Spec. Top. **229**(22–23), 3319–3340 (2020). https://doi.org/10.1140/epjst/e2020-000064-6. arXiv:2006.08782 [hep-ph]
3. C.D. Roberts, Empirical consequences of emergent mass. Symmetry **12**(9), 1468 (2020). https://doi.org/10.3390/sym12091468. arXiv:2009.04011 [hep-ph]
4. C.D. Roberts, On mass and matter. AAPPS Bull. **31**, 6 (2021). https://doi.org/10.1007/s43673-021-00005-4. arXiv:2101.08340 [hep-ph]
5. C.D. Roberts, D.G. Richards, T. Horn, L. Chang, Insights into the emergence of mass from studies of pion and kaon structure. Prog. Part. Nucl. Phys. **120**, 103883 (2021). https://doi.org/10.1016/j.ppnp.2021.103883. arXiv:2102.01765 [hep-ph]
6. D. Binosi, Emergent hadron mass in strong dynamics. Few Body Syst. **63**(2), 42 (2022). https://doi.org/10.1007/s00601-022-01740-6. arXiv:2203.00942 [hep-ph]
7. J. Papavassiliou, Emergence of mass in the gauge sector of QCD*. Chin. Phys. C **46**(11), 112001 (2022). https://doi.org/10.1088/1674-1137/ac84ca. arXiv:2207.04977 [hep-ph]
8. M. Ding, C.D. Roberts, S.M. Schmidt, Emergence of hadron mass and structure. Particles **6**, 57–120 (2023). arXiv:2211.07763 [hep-ph]
9. C.D. Roberts, Origin of the Proton Mass (2022)
10. J.E. Mandula, M. Ogilvie, The gluon is massive: a lattice calculation of the gluon propagator in the Landau gauge. Phys. Lett. B **185**, 127–132 (1987). https://doi.org/10.1016/0370-2693(87)91541-3
11. P.O. Bowman, U.M. Heller, A.G. Williams, Lattice quark propagator with staggered quarks in Landau and Laplacian gauges. Phys. Rev. D **66**, 014505 (2002). https://doi.org/10.1103/PhysRevD.66.014505. arXiv:hep-lat/0203001
12. J.I. Skullerud, P.O. Bowman, A. Kizilersu, D.B. Leinweber, A.G. Williams, Nonperturbative structure of the quark gluon vertex. J. High Energy Phys. **04**, 047 (2003). https://doi.org/10.1088/1126-6708/2003/04/047. arXiv:hep-ph/0303176 [hep-ph]
13. A. Cucchieri, A. Maas, T. Mendes, Exploratory study of three-point Green's functions in Landau-gauge Yang-Mills theory. Phys. Rev. **D74**, 014503 (2006). https://doi.org/10.1103/PhysRevD.74.014503. arXiv:hep-lat/0605011 [hep-lat]
14. E.-M. Ilgenfritz, M. Muller-Preussker, A. Sternbeck, A. Schiller, I.L. Bogolubsky, Landau gauge gluon and ghost propagators from lattice QCD. Braz.J. Phys. **37**, 193–200 (2007). https://doi.org/10.1590/S0103-97332007000200006. arXiv:hep-lat/0609043 [hep-lat]
15. A. Sternbeck, The Infrared behavior of lattice QCD Green's functions. Ph.D. thesis, Humboldt-University Berlin (2006)

16. W. Kamleh, P.O. Bowman, D.B. Leinweber, A.G. Williams, J. Zhang, Unquenching effects in the quark and gluon propagator. Phys. Rev. D **76**, 094501 (2007). https://doi.org/10.1103/PhysRevD.76.094501. arXiv:0705.4129 [hep-lat]
17. A. Cucchieri, T. Mendes, What's up with IR gluon and ghost propagators in Landau gauge? A puzzling answer from huge lattices. PoS LATTICE2007, 297 (2007). https://doi.org/10.22323/1.042.0297. arXiv:0710.0412 [hep-lat]
18. A. Cucchieri, T. Mendes, Constraints on the IR behavior of the gluon propagator in Yang–Mills theories. Phys. Rev. Lett. **100**, 241601 (2008). https://doi.org/10.1103/PhysRevLett.100.241601. arXiv:0712.3517 [hep-lat]
19. I.L. Bogolubsky, E.M. Ilgenfritz, M. Muller-Preussker, A. Sternbeck, The Landau gauge gluon and ghost propagators in 4D SU(3) gluodynamics in large lattice volumes. PoS LATTICE2007, 290 (2007). https://doi.org/10.22323/1.042.0290. arXiv:0710.1968 [hep-lat]
20. A. Cucchieri, A. Maas, T. Mendes, Three-point vertices in Landau-gauge Yang–Mills theory. Phys. Rev. D **77**, 094510 (2008). https://doi.org/10.1103/PhysRevD.77.094510. arXiv:0803.1798 [hep-lat]
21. A. Cucchieri, T. Mendes, Constraints on the IR behavior of the ghost propagator in Yang–Mills theories. Phys. Rev. D **78**, 094503 (2008). https://doi.org/10.1103/PhysRevD.78.094503. arXiv:0804.2371 [hep-lat]
22. A. Cucchieri, T. Mendes, Landau-gauge propagators in Yang–Mills theories at beta = 0: massive solution versus conformal scaling. Phys. Rev. D **81**, 016005 (2010). https://doi.org/10.1103/PhysRevD.81.016005. arXiv:0904.4033 [hep-lat]
23. A. Cucchieri, T. Mendes, E.M.S. Santos, Covariant gauge on the lattice: a new implementation. Phys. Rev. Lett. **103**, 141602 (2009). https://doi.org/10.1103/PhysRevLett.103.141602. arXiv:0907.4138 [hep-lat]
24. I.L. Bogolubsky, E.M. Ilgenfritz, M. Muller-Preussker, A. Sternbeck, Lattice gluodynamics computation of Landau gauge Green's functions in the deep infrared. Phys. Lett. B **676**, 69–73 (2009). https://doi.org/10.1016/j.physletb.2009.04.076. arXiv:0901.0736 [hep-lat]
25. O. Oliveira, P.J. Silva, The Lattice infrared Landau gauge gluon propagator: the infinite volume limit. PoS LAT2009, 226 (2009). https://doi.org/10.22323/1.091.0226. arXiv:0910.2897 [hep-lat]
26. A. Cucchieri, T. Mendes, G.M. Nakamura, E.M.S. Santos, Gluon propagators in linear covariant gauge. PoS FACESQCD, 026 (2010). https://doi.org/10.22323/1.117.0026. arXiv:1102.5233 [hep-lat]
27. O. Oliveira, P. Bicudo, Running gluon mass from landau gauge lattice QCD propagator. J. Phys. G **G38**, 045003 (2011). https://doi.org/10.1088/0954-3899/38/4/045003. arXiv:1002.4151 [hep-lat]
28. P. Boucaud, J.P. Leroy, A.L. Yaouanc, J. Micheli, O. Pene, J. Rodriguez-Quintero, The infrared behaviour of the pure Yang–Mills green functions. Few Body Syst. **53**, 387–436 (2012). https://doi.org/10.1007/s00601-011-0301-2. arXiv:1109.1936 [hep-ph]
29. A. Ayala, A. Bashir, D. Binosi, M. Cristoforetti, J. Rodriguez-Quintero, Quark flavour effects on gluon and ghost propagators. Phys. Rev. D **86**, 074512 (2012). https://doi.org/10.1103/PhysRevD.86.074512. arXiv:1208.0795 [hep-ph]
30. O. Oliveira, P.J. Silva, The lattice Landau gauge gluon propagator: lattice spacing and volume dependence. Phys. Rev. D **86**, 114513 (2012). https://doi.org/10.1103/PhysRevD.86.114513. arXiv:1207.3029 [hep-lat]
31. A. Sternbeck, M. Müller-Preussker, Lattice evidence for the family of decoupling solutions of Landau gauge Yang–Mills theory. Phys. Lett. B **726**, 396–403 (2013). https://doi.org/10.1016/j.physletb.2013.08.017. arXiv:1211.3057 [hep-lat]
32. P. Bicudo, D. Binosi, N. Cardoso, O. Oliveira, P.J. Silva, Lattice gluon propagator in renormalizable ξ gauges. Phys. Rev. D **92**(11), 114514 (2015). https://doi.org/10.1103/PhysRevD.92.114514. arXiv:1505.05897 [hep-lat]
33. A.G. Duarte, O. Oliveira, P.J. Silva, Lattice gluon and ghost propagators, and the strong coupling in pure SU(3) Yang–Mills theory: finite lattice spacing and volume effects. Phys. Rev. D **94**(1), 014502 (2016). https://doi.org/10.1103/PhysRevD.94.014502. arXiv:1605.00594 [hep-lat]
34. A. Athenodorou, D. Binosi, P. Boucaud, F. De Soto, J. Papavassiliou, J. Rodriguez-Quintero, S. Zafeiropoulos, On the zero crossing of the three-gluon vertex. Phys. Lett. B **761**, 444–449 (2016). https://doi.org/10.1016/j.physletb.2016.08.065. arXiv:1607.01278 [hep-ph]
35. A.G. Duarte, O. Oliveira, P.J. Silva, Further evidence for zero crossing on the three gluon vertex. Phys. Rev. D **94**(7), 074502 (2016). https://doi.org/10.1103/PhysRevD.94.074502. arXiv:1607.03831 [hep-lat]
36. O. Oliveira, A. Kizilersu, P.J. Silva, J.-I. Skullerud, A. Sternbeck, A.G. Williams, Lattice Landau gauge quark propagator and the quark-gluon vertex. Acta Phys. Polon. Supp. **9**, 363–368 (2016). https://doi.org/10.5506/APhysPolBSupp.9.363. arXiv:1605.09632 [hep-lat]
37. P. Boucaud, F. De Soto, J. Rodríguez-Quintero, S. Zafeiropoulos, Refining the detection of the zero crossing for the three-gluon vertex in symmetric and asymmetric momentum subtraction schemes. Phys. Rev. D **95**(11), 114503 (2017). https://doi.org/10.1103/PhysRevD.95.114503. arXiv:1701.07390 [hep-lat]
38. A. Sternbeck, P.-H. Balduf, A. Kizilersu, O. Oliveira, P.J. Silva, J.-I. Skullerud, A.G Williams, Triple-gluon and quark-gluon vertex from lattice QCD in Landau gauge. PoS LATTICE2016, 349 (2017). https://doi.org/10.22323/1.256.0349. arXiv:1702.00612 [hep-lat]
39. P. Boucaud, F. De Soto, K. Raya, J. Rodríguez-Quintero, S. Zafeiropoulos, Discretization effects on renormalized gauge-field Green's functions, scale setting, and the gluon mass. Phys. Rev. D **98**(11), 114515 (2018). https://doi.org/10.1103/PhysRevD.98.114515. arXiv:1809.05776 [hep-ph]
40. A. Cucchieri, D. Dudal, T. Mendes, O. Oliveira, M. Roelfs, P.J. Silva, Lattice computation of the ghost propagator in linear covariant gauges. PoS LATTICE2018, 252 (2018). https://doi.org/10.22323/1.334.0252. arXiv:1811.11521 [hep-lat]
41. A. Cucchieri, D. Dudal, T. Mendes, O. Oliveira, M. Roelfs, P.J. Silva, Faddeev-Popov matrix in linear covariant gauge: first results. Phys. Rev. D **98**(9), 091504 (2018). https://doi.org/10.1103/PhysRevD.98.091504. arXiv:1809.08224 [hep-lat]
42. O. Oliveira, P.J. Silva, J.-I. Skullerud, A. Sternbeck, Quark propagator with two flavors of O(a)-improved Wilson fermions. Phys. Rev. D **99**(9), 094506 (2019). https://doi.org/10.1103/PhysRevD.99.094506. arXiv:1809.02541 [hep-lat]
43. D. Dudal, O. Oliveira, P.J. Silva, High precision statistical Landau gauge lattice gluon propagator computation vs. the Gribov–Zwanziger approach. Ann. Phys. **397**, 351–364 (2018). https://doi.org/10.1016/j.aop.2018.08.019. arXiv:1803.02281 [hep-lat]
44. M. Vujinovic, T. Mendes, Probing the tensor structure of lattice three-gluon vertex in Landau gauge. Phys. Rev. D **99**(3), 034501 (2019). https://doi.org/10.1103/PhysRevD.99.034501. arXiv:1807.03673 [hep-lat]

45. Z.-F. Cui, J.-L. Zhang, D. Binosi, F. Soto, C. Mezrag, J. Papavassiliou, C.D. Roberts, J. Rodríguez-Quintero, J. Segovia, S. Zafeiropoulos, Effective charge from lattice QCD. Chin. Phys. C **44**(8), 083102 (2020). https://doi.org/10.1088/1674-1137/44/8/083102. arXiv:1912.08232 [hep-ph]
46. S. Zafeiropoulos, P. Boucaud, F. De Soto, J. Rodríguez-Quintero, J. Segovia, Strong running coupling from the gauge sector of domain wall lattice QCD with physical quark masses. Phys. Rev. Lett. **122**(16), 162002 (2019). https://doi.org/10.1103/PhysRevLett.122.162002. arXiv:1902.08148 [hep-ph]
47. A.C. Aguilar, F. De Soto, M.N. Ferreira, J. Papavassiliou, J. Rodríguez-Quintero, S. Zafeiropoulos, Gluon propagator and three-gluon vertex with dynamical quarks. Eur. Phys. J. C **80**(2), 154 (2020). https://doi.org/10.1140/epjc/s10052-020-7741-0. arXiv:1912.12086 [hep-ph]
48. Maas, A., Vujinović, M.: More on the three-gluon vertex in SU(2) Yang–Mills theory in three and four dimensions. SciPost Phys. Core **5**, 019 (2022). https://doi.org/10.21468/SciPostPhysCore.5.2.019. arXiv:2006.08248 [hep-lat]
49. A. Kızılersü, O. Oliveira, P.J. Silva, J.-I. Skullerud, A. Sternbeck, Quark-gluon vertex from Nf=2 lattice QCD. Phys. Rev. D **103**(11), 114515 (2021). https://doi.org/10.1103/PhysRevD.103.114515. arXiv:2103.02945 [hep-lat]
50. A.C. Aguilar, F. De Soto, M.N. Ferreira, J. Papavassiliou, J. Rodríguez-Quintero, Infrared facets of the three-gluon vertex. Phys. Lett. B **818**, 136352 (2021). https://doi.org/10.1016/j.physletb.2021.136352. arXiv:2102.04959 [hep-ph]
51. A.C. Aguilar, C.O. Ambrósio, F. De Soto, M.N. Ferreira, B.M. Oliveira, J. Papavassiliou, J. Rodríguez-Quintero, Ghost dynamics in the soft gluon limit. Phys. Rev. D **104**(5), 054028 (2021). https://doi.org/10.1103/PhysRevD.104.054028. arXiv:2107.00768 [hep-ph]
52. F. Pinto-Gómez, F. De Soto, M.N. Ferreira, J. Papavassiliou, J. Rodríguez-Quintero, Lattice three-gluon vertex in extended kinematics: planar degeneracy. Phys. Lett. B **838**, 137737 (2023). https://doi.org/10.1016/j.physletb.2023.137737. arXiv:2208.01020 [hep-ph]
53. F. Pinto-Gomez, F. Soto, Three-gluon vertex in Landau-gauge from quenched-lattice QCD in general kinematics. EPJ Web Conf. **274**, 02012 (2022). https://doi.org/10.1051/epjconf/202227402012. arXiv:2211.12199 [hep-lat]
54. F. Pinto-Gómez, F. De Soto, M.N. Ferreira, J. Papavassiliou, J. Rodríguez-Quintero, General kinematics three-gluon vertex in Landau-gauge from quenched-lattice. QCD. PoS LATTICE **2022**, 382 (2023). https://doi.org/10.22323/1.430.0382
55. S.-X. Qin, C.D. Roberts, Impressions of the continuum bound state problem in QCD. Chin. Phys. Lett. **37**(12), 121201 (2020). https://doi.org/10.1088/0256-307X/37/12/121201. arXiv:2008.07629 [hep-ph]
56. Z.-F. Cui, M. Ding, F. Gao, K. Raya, D. Binosi, L. Chang, C.D. Roberts, J. Rodríguez-Quintero, S.M. Schmidt, Kaon and pion Parton distributions. Eur. Phys. J. C **80**(11), 1064 (2020). https://doi.org/10.1140/epjc/s10052-020-08578-4
57. L. Chang, C.D. Roberts, Regarding the distribution of glue in the pion. Chin. Phys. Lett. **38**(8), 081101 (2021). https://doi.org/10.1088/0256-307X/38/8/081101. arXiv:2106.08451 [hep-ph]
58. Z.-F. Cui, M. Ding, J.M. Morgado, K. Raya, D. Binosi, L. Chang, F. De Soto, C.D. Roberts, J. Rodríguez-Quintero, S.M. Schmidt, Emergence of pion Parton distributions. Phys. Rev. D **105**(9), 091502 (2022). https://doi.org/10.1103/PhysRevD.105.L091502. arXiv:2201.00884 [hep-ph]
59. Y. Lu, L. Chang, K. Raya, C.D. Roberts, J. Rodríguez-Quintero, Proton and pion distribution functions in counterpoint. Phys. Lett. B **830**, 137130 (2022). https://doi.org/10.1016/j.physletb.2022.137130. arXiv:2203.00753 [hep-ph]
60. C.D. Roberts, A.G. Williams, Dyson–Schwinger equations and their application to hadronic physics. Prog. Part. Nucl. Phys. **33**, 477–575 (1994). https://doi.org/10.1016/0146-6410(94)90049-3. arXiv:hep-ph/9403224
61. R. Alkofer, L. Smekal, The infrared behavior of QCD Green's functions: confinement dynamical symmetry breaking, and hadrons as relativistic bound states. Phys. Rep. **353**, 281 (2001). https://doi.org/10.1016/S0370-1573(01)00010-2. arXiv:hep-ph/0007355
62. C.S. Fischer, Infrared properties of QCD from Dyson–Schwinger equations. J. Phys. G **32**, 253–291 (2006). https://doi.org/10.1088/0954-3899/32/8/R02. arXiv:hep-ph/0605173
63. C.D. Roberts, Hadron properties and Dyson–Schwinger equations. Prog. Part. Nucl. Phys. **61**, 50–65 (2008). https://doi.org/10.1016/j.ppnp.2007.12.034. arXiv:0712.0633 [nucl-th]
64. D. Binosi, J. Papavassiliou, Pinch technique: theory and applications. Phys. Rep. **479**, 1–152 (2009). https://doi.org/10.1016/j.physrep.2009.05.001. arXiv:0909.2536 [hep-ph]
65. A. Bashir, L. Chang, I.C. Cloet, B. El-Bennich, Y.-X. Liu et al., Collective perspective on advances in Dyson–Schwinger Equation QCD. Commun. Theor. Phys. **58**, 79–134 (2012). https://doi.org/10.1088/0253-6102/58/1/16. arXiv:1201.3366 [nucl-th]
66. D. Binosi, L. Chang, J. Papavassiliou, C.D. Roberts, Bridging a gap between continuum-QCD and ab initio predictions of hadron observables. Phys. Lett. B **742**, 183–188 (2015). https://doi.org/10.1016/j.physletb.2015.01.031. arXiv:1412.4782 [nucl-th]
67. I.C. Cloet, C.D. Roberts, Explanation and prediction of observables using continuum strong QCD. Prog. Part. Nucl. Phys. **77**, 1–69 (2014). https://doi.org/10.1016/j.ppnp.2014.02.001. arXiv:1310.2651 [nucl-th]
68. A.C. Aguilar, D. Binosi, J. Papavassiliou, The gluon mass generation mechanism: a concise primer. Front. Phys. (Beijing) **11**(2), 111203 (2016). https://doi.org/10.1007/s11467-015-0517-6. arXiv:1511.08361 [hep-ph]
69. D. Binosi, L. Chang, J. Papavassiliou, S.-X. Qin, C.D. Roberts, Symmetry preserving truncations of the gap and Bethe–Salpeter equations. Phys. Rev. D **93**(9), 096010 (2016). https://doi.org/10.1103/PhysRevD.93.096010. arXiv:1601.05441 [nucl-th]
70. D. Binosi, C. Mezrag, J. Papavassiliou, C.D. Roberts, J. Rodriguez-Quintero, Process-independent strong running coupling. Phys. Rev. D **96**(5), 054026 (2017). https://doi.org/10.1103/PhysRevD.96.054026. arXiv:1612.04835 [nucl-th]
71. M.Q. Huber, Nonperturbative properties of Yang–Mills theories. Phys. Rep. **879**, 1–92 (2020). https://doi.org/10.1016/j.physrep.2020.04.004. arXiv:1808.05227 [hep-ph]
72. J.M. Pawlowski, D.F. Litim, S. Nedelko, L. Smekal, Infrared behavior and fixed points in Landau gauge QCD. Phys. Rev. Lett. **93**, 152002 (2004). https://doi.org/10.1103/PhysRevLett.93.152002. arXiv:hep-th/0312324 [hep-th]
73. J.M. Pawlowski, Aspects of the functional renormalisation group. Ann. Phys. **322**, 2831–2915 (2007). https://doi.org/10.1016/j.aop.2007.01.007. arXiv:hep-th/0512261 [hep-th]

74. C.S. Fischer, A. Maas, J.M. Pawlowski, On the infrared behavior of Landau gauge Yang–Mills theory. Ann. Phys. **324**, 2408–2437 (2009). https://doi.org/10.1016/j.aop.2009.07.009. arXiv:0810.1987 [hep-ph]
75. M.E. Carrington, Renormalization group flow equations connected to the n-particle-irreducible effective action. Phys. Rev. D **87**(4), 045011 (2013). https://doi.org/10.1103/PhysRevD.87.045011. arXiv:1211.4127 [hep-ph]
76. M.E. Carrington, W.-J. Fu, D. Pickering, J.W. Pulver, Renormalization group methods and the 2PI effective action. Phys. Rev. D **91**(2), 025003 (2015). https://doi.org/10.1103/PhysRevD.91.025003. arXiv:1404.0710 [hep-ph]
77. A.K. Cyrol, M. Mitter, J.M. Pawlowski, N. Strodthoff, Nonperturbative quark, gluon, and meson correlators of unquenched QCD. Phys. Rev. D **97**(5), 054006 (2018). https://doi.org/10.1103/PhysRevD.97.054006. arXiv:1706.06326 [hep-ph]
78. L. Corell, A.K. Cyrol, M. Mitter, J.M. Pawlowski, N. Strodthoff, Correlation functions of three-dimensional Yang–Mills theory from the FRG. SciPost Phys. **5**(6), 066 (2018). https://doi.org/10.21468/SciPostPhys.5.6.066. arXiv:1803.10092 [hep-ph]
79. M.Q. Huber, Correlation functions of Landau gauge Yang–Mills theory. Phys. Rev. D **101**, 114009 (2020). https://doi.org/10.1103/PhysRevD.101.114009. arXiv:2003.13703 [hep-ph]
80. N. Dupuis, L. Canet, A. Eichhorn, W. Metzner, J.M. Pawlowski, M. Tissier, N. Wschebor, The nonperturbative functional renormalization group and its applications. Phys. Rep. **910**, 1–114 (2021). https://doi.org/10.1016/j.physrep.2021.01.001. arXiv:2006.04853 [cond-mat.stat-mech]
81. J.-P. Blaizot, J.M. Pawlowski, U. Reinosa, Functional renormalization group and 2PI effective action formalism. Ann. Phys. **431**, 168549 (2021). https://doi.org/10.1016/j.aop.2021.168549. arXiv:2102.13628 [hep-th]
82. J.M. Pawlowski, C.S. Schneider, N. Wink, On gauge consistency in gauge-fixed Yang–Mills theory (2022). arXiv:2202.11123 [hep-th]
83. J. Horak, F. Ihssen, J. Papavassiliou, J.M. Pawlowski, A. Weber, C. Wetterich, Gluon condensates and effective gluon mass. SciPost Phys. **13**(2), 042 (2022). https://doi.org/10.21468/SciPostPhys.13.2.042. arXiv:2201.09747 [hep-ph]
84. J.M. Cornwall, Quark confinement and vortices in massive gauge invariant QCD. Nucl. Phys. B **157**, 392 (1979)
85. G. Parisi, R. Petronzio, On low-energy tests of QCD. Phys. Lett. B **94**, 51 (1980)
86. J.M. Cornwall, Dynamical mass generation in continuum QCD. Phys. Rev. D **26**, 1453 (1982). https://doi.org/10.1103/PhysRevD.26.1453
87. C.W. Bernard, Monte Carlo evaluation of the effective gluon mass. Phys. Lett. B **108**, 431–434 (1982). https://doi.org/10.1016/0370-2693(82)91228-X
88. C.W. Bernard, Adjoint Wilson lines and the effective gluon mass. Nucl. Phys. B **219**, 341–357 (1983). https://doi.org/10.1016/0550-3213(83)90645-4
89. J.F. Donoghue, The gluon 'mass' in the bag model. Phys. Rev. D **29**, 2559 (1984). https://doi.org/10.1103/PhysRevD.29.2559
90. S.J. Brodsky, R. Shrock, Maximum wavelength of confined quarks and gluons and properties of quantum chromodynamics. Phys. Lett. B **666**, 95–99 (2008). https://doi.org/10.1016/j.physletb.2008.06.054. arXiv:0806.1535 [hep-th]
91. J. Braun, H. Gies, J.M. Pawlowski, Quark confinement from color confinement. Phys. Lett. B **684**, 262–267 (2010). https://doi.org/10.1016/j.physletb.2010.01.009. arXiv:0708.2413 [hep-th]
92. F. Gao, S.-X. Qin, C.D. Roberts, J. Rodriguez-Quintero, Locating the Gribov horizon. Phys. Rev. D **97**(3), 034010 (2018). https://doi.org/10.1103/PhysRevD.97.034010. arXiv:1706.04681 [hep-ph]
93. J. Meyers, E.S. Swanson, Spin zero glueballs in the Bethe–Salpeter formalism. Phys. Rev. D **87**(3), 036009 (2013). https://doi.org/10.1103/PhysRevD.87.036009. arXiv:1211.4648 [hep-ph]
94. H. Sanchis-Alepuz, C.S. Fischer, C. Kellermann, L. Smekal, Glueballs from the Bethe–Salpeter equation. Phys. Rev. D **92**, 034001 (2015). https://doi.org/10.1103/PhysRevD.92.034001. arXiv:1503.06051 [hep-ph]
95. E.V. Souza, M.N. Ferreira, A.C. Aguilar, J. Papavassiliou, C.D. Roberts, S.-S. Xu, Pseudoscalar glueball mass: a window on three-gluon interactions. Eur. Phys. J. A **56**(1), 25 (2020). https://doi.org/10.1140/epja/s10050-020-00041-y. arXiv:1909.05875 [nucl-th]
96. M.Q. Huber, C.S. Fischer, H. Sanchis-Alepuz, Spectrum of scalar and pseudoscalar glueballs from functional methods. Eur. Phys. J. C **80**(11), 1077 (2020). https://doi.org/10.1140/epjc/s10052-020-08649-6. arXiv:2004.00415 [hep-ph]
97. M.Q. Huber, C.S. Fischer, H. Sanchis-Alepuz, Higher spin glueballs from functional methods. Eur. Phys. J. C **81**(12), 1083 (2021) https://doi.org/10.1140/epjc/s10052-021-09864-5. arXiv:2110.09180 [hep-ph]. [Erratum: Eur. Phys. J. C **82**, 38 (2022)]
98. J.S. Schwinger, Gauge invariance and mass. Phys. Rev. **125**, 397–398 (1962). https://doi.org/10.1103/PhysRev.125.397
99. J.S. Schwinger, Gauge invariance and mass. 2. Phys. Rev. **128**, 2425–2429 (1962). https://doi.org/10.1103/PhysRev.128.2425
100. R. Jackiw, K. Johnson, Dynamical model of spontaneously broken gauge symmetries. Phys. Rev. D **8**, 2386–2398 (1973). https://doi.org/10.1103/PhysRevD.8.2386
101. Jackiw, R.: Dynamical symmetry breaking, in **Erice 1973, Proceedings, Laws Of Hadronic Matter*, New York 1975, 225–251 and MIT Cambridge—COO-3069-190 (73,REC.AUG 74)* (1973)
102. J.M. Cornwall, R.E. Norton, Spontaneous symmetry breaking without scalar mesons. Phys. Rev. D **8**, 3338–3346 (1973). https://doi.org/10.1103/PhysRevD.8.3338
103. E. Eichten, F. Feinberg, Dynamical symmetry breaking of nonabelian gauge symmetries. Phys. Rev. D **10**, 3254–3279 (1974). https://doi.org/10.1103/PhysRevD.10.3254
104. J. Smit, On the possibility that massless Yang–Mills fields generate massive vector particles. Phys. Rev. D **10**, 2473 (1974). https://doi.org/10.1103/PhysRevD.10.2473
105. E.C. Poggio, E. Tomboulis, S.-H.H. Tye, Dynamical symmetry breaking in nonabelian field theories. Phys. Rev. D **11**, 2839 (1975). https://doi.org/10.1103/PhysRevD.11.2839
106. J. Papavassiliou, Gauge invariant proper selfenergies and vertices in gauge theories with broken symmetry. Phys. Rev. D **41**, 3179 (1990). https://doi.org/10.1103/PhysRevD.41.3179

107. A.C. Aguilar, D. Binosi, J. Papavassiliou, Gluon and ghost propagators in the Landau gauge: deriving lattice results from Schwinger–Dyson equations. Phys. Rev. D **78**, 025010 (2008). https://doi.org/10.1103/PhysRevD.78.025010. arXiv:0802.1870 [hep-ph]
108. A.C. Aguilar, D. Ibanez, V. Mathieu, J. Papavassiliou, Massless bound-state excitations and the Schwinger mechanism in QCD. Phys. Rev. D **85**, 014018 (2012). https://doi.org/10.1103/PhysRevD.85.014018. arXiv:1110.2633 [hep-ph]
109. A.C. Aguilar, D. Binosi, J. Papavassiliou, The dynamical equation of the effective gluon mass. Phys. Rev. D **84**, 085026 (2011). https://doi.org/10.1103/PhysRevD.84.085026. arXiv:1107.3968 [hep-ph]
110. D. Ibañez, J. Papavassiliou, Gluon mass generation in the massless bound-state formalism. Phys. Rev. D **87**(3), 034008 (2013). https://doi.org/10.1103/PhysRevD.87.034008. arXiv:1211.5314 [hep-ph]
111. D. Binosi, D. Ibañez, J. Papavassiliou, The all-order equation of the effective gluon mass. Phys. Rev. D **86**, 085033 (2012). https://doi.org/10.1103/PhysRevD.86.085033. arXiv:1208.1451 [hep-ph]
112. A.C. Aguilar, D. Binosi, J. Papavassiliou, Unquenching the gluon propagator with Schwinger–Dyson equations. Phys. Rev. D **86**, 014032 (2012). https://doi.org/10.1103/PhysRevD.86.014032. arXiv:1204.3868 [hep-ph]
113. A.C. Aguilar, D. Binosi, C.T. Figueiredo, J. Papavassiliou, Unified description of seagull cancellations and infrared finiteness of gluon propagators. Phys. Rev. D **94**(4), 045002 (2016). https://doi.org/10.1103/PhysRevD.94.045002. arXiv:1604.08456 [hep-ph]
114. A.C. Aguilar, D. Binosi, J. Papavassiliou, Schwinger mechanism in linear covariant gauges. Phys. Rev. D **95**(3), 034017 (2017). https://doi.org/10.1103/PhysRevD.95.034017. arXiv:1611.02096 [hep-ph]
115. G. Eichmann, J.M. Pawlowski, J.M. Silva, Mass generation in Landau-gauge Yang–Mills theory. Phys. Rev. D **104**(11), 114016 (2021). https://doi.org/10.1103/PhysRevD.104.114016. arXiv:2107.05352 [hep-ph]
116. A.C. Aguilar, M.N. Ferreira, J. Papavassiliou, Exploring smoking-gun signals of the Schwinger mechanism in QCD. Phys. Rev. D **105**(1), 014030 (2022). https://doi.org/10.1103/PhysRevD.105.014030. arXiv:2111.09431 [hep-ph]
117. A.C. Aguilar, F. De Soto, M.N. Ferreira, J. Papavassiliou, F. Pinto-Gómez, C.D. Roberts, J. Rodríguez-Quintero, Schwinger mechanism for gluons from lattice QCD (2022). arXiv:2211.12594 [hep-ph]
118. M.N. Ferreira, J. Papavassiliou, Gauge sector dynamics in QCD. Particles **6**(1), 312–363 (2023). https://doi.org/10.3390/particles6010017. arXiv:2301.02314 [hep-ph]
119. A.C. Aguilar, D. Binosi, J. Papavassiliou, Gluon mass through ghost synergy. J. High Energy Phys. **01**, 050 (2012). https://doi.org/10.1007/JHEP01(2012)050. arXiv:1108.5989 [hep-ph]
120. A.C. Aguilar, D. Binosi, J. Papavassiliou, Gluon mass generation in the presence of dynamical quarks. Phys. Rev. D **88**, 074010 (2013). https://doi.org/10.1103/PhysRevD.88.074010. arXiv:1304.5936 [hep-ph]
121. A.C. Aguilar, D. Binosi, C.T. Figueiredo, J. Papavassiliou, Evidence of ghost suppression in gluon mass scale dynamics. Eur. Phys. J. C **78**(3), 181 (2018). https://doi.org/10.1140/epjc/s10052-018-5679-2. arXiv:1712.06926 [hep-ph]
122. B.S. DeWitt, Quantum theory of gravity. 2. The manifestly covariant theory. Phys. Rev. **162**, 1195–1239 (1967). https://doi.org/10.1103/PhysRev.162.1195
123. G. Hooft, Renormalizable Lagrangians for massive Yang–Mills fields. Nucl. Phys. B **35**, 167–188 (1971). https://doi.org/10.1016/0550-3213(71)90139-8
124. J. Honerkamp, The question of invariant renormalizability of the massless Yang–Mills theory in a manifest covariant approach. Nucl. Phys. B **48**, 269–287 (1972). https://doi.org/10.1016/0550-3213(72)90063-6
125. R.E. Kallosh, The renormalization in nonabelian gauge theories. Nucl. Phys. B **78**, 293–312 (1974). https://doi.org/10.1016/0550-3213(74)90284-3
126. H. Kluberg-Stern, J.B. Zuber, Renormalization of nonabelian gauge theories in a background field gauge. 1. Green functions. Phys. Rev. D **12**, 482–488 (1975). https://doi.org/10.1103/PhysRevD.12.482
127. I.Y. Arefeva, L.D. Faddeev, A.A. Slavnov, Generating functional for the s matrix in gauge theories. Teor. Mat. Fiz. **21**, 311–321 (1974). https://doi.org/10.1007/BF01038094
128. L.F. Abbott, The background field method beyond one loop. Nucl. Phys. B **185**, 189–203 (1981). https://doi.org/10.1016/0550-3213(81)90371-0
129. S. Weinberg, Effective gauge theories. Phys. Lett. B **91**, 51–55 (1980). https://doi.org/10.1016/0370-2693(80)90660-7
130. L.F. Abbott, Introduction to the background field method. Acta Phys. Polon. B **13**, 33 (1982)
131. G.M. Shore, Symmetry restoration and the background field method in gauge theories. Ann. Phys. **137**, 262 (1981). https://doi.org/10.1016/0003-4916(81)90198-6
132. L.F. Abbott, M.T. Grisaru, R.K. Schaefer, The background field method and the S matrix. Nucl. Phys. B **229**, 372–380 (1983). https://doi.org/10.1016/0550-3213(83)90337-1
133. J.C. Taylor, Ward identities and charge renormalization of the Yang–Mills field. Nucl. Phys. B **33**, 436–444 (1971). https://doi.org/10.1016/0550-3213(71)90297-5
134. A.A. Slavnov, Ward identities in gauge theories. Theor. Math. Phys. **10**, 99–107 (1972). https://doi.org/10.1007/BF01090719
135. J.M. Cornwall, J. Papavassiliou, Gauge invariant three gluon vertex in QCD. Phys. Rev. D **40**, 3474 (1989). https://doi.org/10.1103/PhysRevD.40.3474
136. A.C. Aguilar, J. Papavassiliou, Gluon mass generation in the PT-BFM scheme. J. High Energy Phys. **12**, 012 (2006). https://doi.org/10.1088/1126-6708/2006/12/012. arXiv:hep-ph/0610040
137. J.S. Ball, T.-W. Chiu, Analytic properties of the vertex function in gauge theories. 2. Phys. Rev. D **22**, 2550 (1980). https://doi.org/10.1103/PhysRevD.22.2550 . [Erratum: Phys. Rev. D **23**, 3085 (1981)]
138. A.I. Davydychev, P. Osland, O.V. Tarasov, Three gluon vertex in arbitrary gauge and dimension. Phys. Rev. D **54**, 4087–4113 (1996). https://doi.org/10.1103/PhysRevD.59.109901 arXiv:hep-ph/9605348. [Erratum: Phys. Rev. D **59**, 109901 (1999)]
139. Smekal, L., Hauck, A., Alkofer, R.: A solution to coupled Dyson–Schwinger equations for gluons and ghosts in landau gauge. Ann. Phys. **267**, 1–60 (1998). https://doi.org/10.1006/aphy.1998.5806. https://doi.org/10.1006/aphy.1998.5864. arXiv:hep-ph/9707327 [hep-ph]. [Erratum: Ann. Phys. **269**, 182(1998)]
140. D. Binosi, J. Papavassiliou, Gauge invariant Ansatz for a special three-gluon vertex. J. High Energy Phys. **03**, 121 (2011). https://doi.org/10.1007/JHEP03(2011)121. arXiv:1102.5662 [hep-ph]

141. J.A. Gracey, H. Kißler, D. Kreimer, Self-consistency of off-shell Slavnov–Taylor identities in QCD. Phys. Rev. D **100**(8), 085001 (2019). https://doi.org/10.1103/PhysRevD.100.085001. arXiv:1906.07996 [hep-th]
142. A.C. Aguilar, M.N. Ferreira, C.T. Figueiredo, J. Papavassiliou, Nonperturbative structure of the ghost-gluon kernel. Phys. Rev. D **99**, 034026 (2019). https://doi.org/10.1103/PhysRevD.99.034026. arXiv:1811.08961 [hep-ph]
143. D. Dudal, J.A. Gracey, S.P. Sorella, N. Vandersickel, H. Verschelde, A refinement of the Gribov–Zwanziger approach in the Landau gauge: infrared propagators in harmony with the lattice results. Phys. Rev. D **78**, 065047 (2008). https://doi.org/10.1103/PhysRevD.78.065047. arXiv:0806.4348 [hep-th]
144. P. Boucaud, J.P. Leroy, A.L.Y. J. Micheli, O. Pène, J. Rodríguez-Quintero, On the IR behaviour of the Landau-gauge ghost propagator. J. High Energy Phys. **06**, 099 (2008). https://doi.org/10.1088/1126-6708/2008/06/099. arXiv:0803.2161 [hep-ph]
145. P. Boucaud, J.-P. Leroy, A.L. Yaouanc, J. Micheli, O. Pene et al., IR finiteness of the ghost dressing function from numerical resolution of the ghost SD equation. J. High Energy Phys. **06**, 012 (2008). https://doi.org/10.1088/1126-6708/2008/06/012. arXiv:0801.2721 [hep-ph]
146. K.-I. Kondo, Infrared behavior of the ghost propagator in the Landau gauge Yang–Mills theory. Prog. Theor. Phys. **122**, 1455–1475 (2010). https://doi.org/10.1143/PTP.122.1455. arXiv:0907.3249 [hep-th]
147. M.R. Pennington, D.J. Wilson, Are the Dressed Gluon and Ghost Propagators in the Landau Gauge presently determined in the confinement regime of QCD? Phys. Rev. D **84**, 119901 (2011). https://doi.org/10.1103/PhysRevD.84.094028. https://doi.org/10.1103/PhysRevD.84.119901. arXiv:1109.2117 [hep-ph]
148. D. Dudal, O. Oliveira, J. Rodriguez-Quintero, Nontrivial ghost-gluon vertex and the match of RGZ, DSE and lattice Yang–Mills propagators. Phys. Rev. **D86**, 105005 (2012). https://doi.org/10.1103/PhysRevD.86.105005. https://doi.org/10.1103/PhysRevD.86.109902. arXiv:1207.5118 [hep-ph]
149. A.C. Aguilar, D. Ibañez, J. Papavassiliou, Ghost propagator and ghost-gluon vertex from Schwinger–Dyson equations. Phys. Rev. D **87**(11), 114020 (2013). https://doi.org/10.1103/PhysRevD.87.114020. arXiv:1303.3609 [hep-ph]
150. A.K. Cyrol, L. Fister, M. Mitter, J.M. Pawlowski, N. Strodthoff, Landau gauge Yang–Mills correlation functions. Phys. Rev. D **94**(5), 054005 (2016). https://doi.org/10.1103/PhysRevD.94.054005. arXiv:1605.01856 [hep-ph]
151. A.C. Aguilar, M.N. Ferreira, J. Papavassiliou, Novel sum rules for the three-point sector of QCD. Eur. Phys. J. C **80**(9), 887 (2020). https://doi.org/10.1140/epjc/s10052-020-08453-2. arXiv:2006.04587 [hep-ph]
152. M.Q. Huber, On non-primitively divergent vertices of Yang–Mills theory. Eur. Phys. J. C **77**(11), 733 (2017). https://doi.org/10.1140/epjc/s10052-017-5310-y. arXiv:1709.05848 [hep-ph]
153. W. Schleifenbaum, A. Maas, J. Wambach, R. Alkofer, Infrared behaviour of the ghost-gluon vertex in Landau gauge Yang–Mills theory. Phys. Rev. D **72**, 014017 (2005). https://doi.org/10.1103/PhysRevD.72.014017. arXiv:hep-ph/0411052
154. M.Q. Huber, L. Smekal, On the influence of three-point functions on the propagators of Landau gauge Yang–Mills theory. J. High Energy Phys. **04**, 149 (2013). https://doi.org/10.1007/JHEP04(2013)149. arXiv:1211.6092 [hep-th]
155. B.W. Mintz, L.F. Palhares, S.P. Sorella, A.D. Pereira, Ghost-gluon vertex in the presence of the Gribov horizon. Phys. Rev. D **97**(3), 034020 (2018). https://doi.org/10.1103/PhysRevD.97.034020. arXiv:1712.09633 [hep-th]
156. A.C. Aguilar, M.N. Ferreira, C.T. Figueiredo, J. Papavassiliou, Nonperturbative Ball–Chiu construction of the three-gluon vertex. Phys. Rev. D **99**(9), 094010 (2019). https://doi.org/10.1103/PhysRevD.99.094010. arXiv:1903.01184 [hep-ph]
157. N. Barrios, M. Peláez, U. Reinosa, N. Wschebor, The ghost-antighost-gluon vertex from the Curci–Ferrari model: two-loop corrections. Phys. Rev. D **102**, 114016 (2020). https://doi.org/10.1103/PhysRevD.102.114016. arXiv:2009.00875 [hep-th]
158. A.C. Aguilar, M.N. Ferreira, J. Papavassiliou, Gluon dynamics from an ordinary differential equation. Eur. Phys. J. C **81**(1), 54 (2021). https://doi.org/10.1140/epjc/s10052-021-08849-8. arXiv:2010.12714 [hep-ph]
159. G. Eichmann, R. Williams, R. Alkofer, M. Vujinovic, The three-gluon vertex in Landau gauge. Phys. Rev. D **89**, 105014 (2014). https://doi.org/10.1103/PhysRevD.89.105014. arXiv:1402.1365 [hep-ph]
160. A. Blum, M.Q. Huber, M. Mitter, L. Smekal, Gluonic three-point correlations in pure Landau gauge QCD. Phys. Rev. D **89**, 061703 (2014). https://doi.org/10.1103/PhysRevD.89.061703. arXiv:1401.0713 [hep-ph]
161. M.Q. Huber, Correlation functions of three-dimensional Yang–Mills theory from Dyson–Schwinger equations. Phys. Rev. D **93**(8), 085033 (2016). https://doi.org/10.1103/PhysRevD.93.085033. arXiv:1602.02038 [hep-th]
162. P.O. Bowman, U.M. Heller, D.B. Leinweber, M.B. Parappilly, A.G. Williams, Unquenched gluon propagator in Landau gauge. Phys. Rev. D **70**, 034509 (2004). https://doi.org/10.1103/PhysRevD.70.034509. arXiv:hep-lat/0402032